Dissociative Phosphoryl Transfer in PEP Mutase Catalysis: Structure of the Enzyme/Sulfopyruvate Complex and Kinetic Properties of Mutants[†,‡]

Sijiu Liu,[§] Zhibing Lu,[#] Yong Jia,[#] Debra Dunaway-Mariano,[#] and Osnat Herzberg*[,§]

Center for Advanced Research in Biotechnology, University of Maryland Biotechnology Institute, 9600 Gudelsky Drive, Rockville, Maryland 20850, and Department of Chemistry, University of New Mexico, Albuquerque, New Mexico 87131

Received April 25, 2002; Revised Manuscript Received May 30, 2002

ABSTRACT: The crystal structure of PEP mutase from *Mytilus edulis* in complex with a substrate-analogue inhibitor, sulfopyruvate S-pyr (K_i = 22 μM), has been determined at 2.25 Å resolution. Mg(II)-S-pyr binds in the α/β barrel's central channel, at the C-termini of the β-strands. The binding mode of S-pyr's pyruvyl moiety resembles the binding mode of oxalate seen earlier. The location of the sulfo group of S-pyr is postulated to mimic the phosphonyl group of the product phosphonopyruvate (P-pyr). This sulfo group interacts with the guanidinium group of Arg159, but it is not aligned for nucleopilic attack by neighboring basic amino side chains. Kinetic analysis of site directed mutants, probing the key active site residues Asp58, Arg159, Asn122, and His190 correlate well with the structural information. The results presented here rule out a phosphoryl transfer mechanism involving a double displacement, and suggest instead that PEP mutase catalysis proceeds via a dissociative mechanism in which the pyruvyl C(3) adds to the same face of the phosphorus from which the C(2)O departs. We propose that Arg159 and His190 serve to hold the phosphoryl/metaphosphate/phosphonyl group stationary along the reaction pathway, while the pyruvyl C(1)−C(2) bond rotates upon formation of the metaphosphate. In agreement with published data, the phosphoryl group transfer occurs on the *Si*-face of PEP with retention of configuration at phosphorus.

We examine here the mechanism of phosphoryl transfer in the conversion of PEP[1] to P-pyr catalyzed by PEP mutase (*1*, *2*):

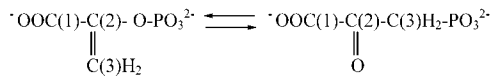

This P−C bond forming reaction serves as the entry point to all known phosphonate biosynthetic pathways (*3*). Despite intense efforts to determine the mechanism of catalysis by this unique enzyme, the pathway for phosphoryl transfer has remained elusive (*4*−*11*). A great deal is known about enzymic and nonenzymic phosphoryl transfer mechanisms (for reviews see refs *12*−*21*), and it is against this backdrop that we present the unusual case of PEP mutase.

A phosphoryl transfer may proceed via one of the following pathways: (i) dissociative, in which a trigonal metaphosphate intermediate is formed, (ii) concerted, associative transfer, involving a trigonal bipyramidal transition state, (iii) stepwise associative transfer (otherwise known as the addition−elimination pathway), involving a trigonal bipyramidal intermediate. While the concerted reaction is thought to proceed with the phosphoryl group donor and acceptor positioned in-line on the trigonal bipyramid apical positions, for the mechanisms involving intermediates, both in-line and adjacent attacks are possible.

The preferred pathway is determined by the nature of the phosphorus electrophile, the nucleophile, and the reaction medium (solvent or enzyme active site) (see for examples, refs *22* and *23*). Knowledge of the stereochemistry of the phosphoryl transfer at phosphorus can aid in the determination of which pathway is operative for a given reaction (see for examples refs *17*, *18*, and *24*). The stereochemistry of phosphoryl transfer in the PEP mutase (measured with the enzyme from *Tetrahymena pyriformis*) is retention (*5*, *6*).

Kinetic isotope effects (*19*, *25*) have also been used as a tool in identifying the phosphoryl transfer reactions, assigning fractional dissociative and associative character to the rate limiting transition state. For phosphate monoesters (such as the substrate of PEP mutase), kinetic isotope effect studies have indicated that phosphoryl transfers proceed through largely dissociative transition states (*19*, *20*).

Retention of configuration in a single phosphoryl transfer step indicates that the nucleophile added to, and the leaving group departed from, the same face of the phosphoryl group (i.e., adjacent associative pathway). This requires pseudorotation at phosphorus to place the leaving group at the apical position. On the other hand, for the dissociative pathway, both faces of the symmetrical metaphosphate are equivalent,

[†] Supported by the NSF grant MCB9813271 (O.H.) and NIH Grant GM36260 (D.D.-M.).

[‡] The coordinates have been deposited in the Protein Data Bank (entry code 1M1B).

* To whom correspondence should be addressed (telephone, 301-738-6245; fax, 301-738-6255; E-mail, osnat@carb.nist.gov).

[§] University of Maryland Biotechnology Institute.

[#] University of New Mexico.

[1] Abbreviations: PEP, phosphoenolpyruvate; P-pyr, phosphonopyruvate; S-pyr, sulfopyruvate; PEP mutase, phosphoenolpyruvate mutase; Hepes, *N*-(2-hydroxyethyl)-piperazine-*N*′-ethanesulfonic acid.

10.1021/bi026024v CCC: $22.00
Published on Web 07/19/2002

and thus racemization is to be expected. Racemization has been demonstrated with much difficulty in solution using chiral phosphate monoesters (*26*, *27*), but has not been observed in enzyme catalyzed phosphoryl reactions. This may be attributed to the geometrical constraints imposed by the immobilization of the reactant pair within the confines of the active site.

Because of the crowded environment at enzyme active sites pseudorotation may be difficult to achieve. The optimal arrangement of the nucleophile relative to the leaving group for substitution at phosphorus is in-line, leading to inversion of stereochemistry independent of whether the mechanism is associative or dissociative. However, retention of configuration is often observed in enzymes. This stereochemistry originates from two in-line sequential displacements, mediated by phosphoenzyme intermediates (viz. side chain of His, Asp, Ser, Thr, Tyr, Cys, or Lys) (*16*).

Retention of configuration observed for the PEP mutase reaction then is consistent with the well precedented associative double-displacement pathway, which in this particular case proceeds via a phosphoenzyme-pyruvate enolate intermediate. However, retention of configuration is also consistent with a novel dissociative pathway involving an enzyme−metaphosphate−pyruvate enolate intermediate. Because the phosphoryl transfer occurs intramolecularly, steric requirements of substrate binding, that would otherwise impede frontal displacement, are not an issue here. In principle, the two mechanisms can be distinguished by rapid quench experiments in which the enzyme is denatured during the course of a single turnover of ^{32}P-labeled PEP. However, neither ^{32}P-labeled enzyme, indicative of the phosphoenzyme intermediate nor $^{32}P_i$, indicative of the metaphosphate intermediate, were detected when such an experiment was carried out (*8*). Attempts to trap the pyruvate enolate as [^{14}C]-pyruvate also failed, indicating that the PEP mutase intermediate does not accumulate to a level sufficient for experimental detection.

A structural-based approach was taken to determine whether the active site contains a nucleophilic residue for in-line attack at phosphorus consistent with the double displacement mechanism. The crystal structure of the PEP mutase from the mollusk *Mytilus edulis* was determined in the presence of Mg(II)-oxalate (*10*), a tight binding competitive inhibitor (K_i = 25−32 μM for the *T. pyriformis* PEP mutase (*7*, *8*) and K_i = 8.4 μM for the *M. edulis* PEP mutase (this work)) analogous to pyruvate enolate. Because oxalate is a symmetrical molecule, the location of the PEP's phosphoryl group could be inferred only by considering the active site environment. In the complex, one carboxylate group of the inhibitor interacts with the guanidinium group of Arg159, and the second carboxylate group is oriented in the opposite direction, toward Asp58 (Figure 1). In modeling PEP binding, the phosphoryl group therefore must be oriented to interact with either the electropositive residue, Arg159, or aligned with the nucleophilic residue, Asp58. Substituting alanine for Arg159 reduced k_{cat} by 4 orders of magnitude, whereas the activity could not be detected in the Asp58 to alanine mutant (*11*). The abolished activity of the D58A mutant enzyme, together with the common occurrence of in-line phosphoryl displacements that utilize phosphoenzyme intermediates favored a mechanism in which Asp58 is the phosphoryl acceptor, and Arg159 forms an ion pair with the pyruvate carboxylate group. An atomic model consistent with this mechanism requires a small shift in the position of Mg−PEP compared with Mg-oxalate, whereas no such shift is necessary for the alternate model in which the PEP phosphoryl group is positioned for interaction with the Arg159.

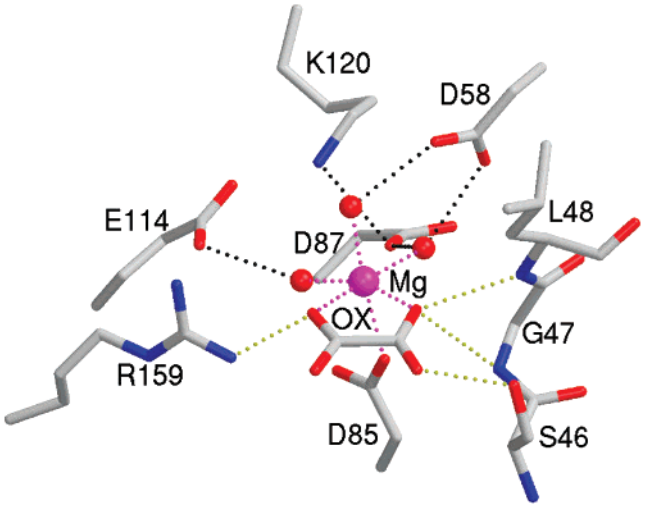

FIGURE 1: Binding of Mg(II)-oxalate to PEP-mutase (*10*). Asp58 and Arg159 are located on opposite sides of the oxalate, and because of the compound's symmetry, it is impossible to conclude which is the key residue that catalyses the phosphotransfer in the true substrate (*10*). Atomic colors are as follows: oxygen − red, carbon − white, Mg^{2+} − magenta. Coordination to the Mg(II) is shown in magenta, electrostatic interactions with oxalate are shown in yellow, and protein interactions with Mg(II)-coordinated water molecules are shown in gray.

The ambiguity of the PEP positioning in the mutase active site prompted a search for a P-pyr analogue that could be used for enzyme cocrystallization. S-pyr is a compound isosteric with P-pyr, with the sulfur replacing phosphorus. In the work presented here, we show that S-pyr is a tight-binding PEP mutase inhibitor, and describe the crystal structure of the enzyme−inhibitor complex. The structure and mutagenesis data are compatible with the dissociative pathway for phosphoryl transfer and incompatible with the double displacement mechanism.

MATERIALS AND METHODS

P-pyr and S-pyr and Enzyme. P-pyr (*28*) and S-pyr (*29*) were prepared according to published procedures. *Mytilus edulis* PEP mutase was purified from the *Escherichia coli* clone as described previously (*11*).

Site-Directed Mutants. Site-directed mutagenesis was carried out using a PCR-based strategy with the YJ102 clone as described previously (*11*). Mutant plasmids isolated from JM109 *E. coli* host cells were subjected to DNA sequencing to verify the correct PEP mutase gene sequence, and then used to transform BL21(DE3) *E. coli* cells for expression. The PEP mutase mutants were purified to homogeneity (as judged by SDS−PAGE analysis) in the same manner used to purify wild-type recombinant PEP mutase. Yields were 5−8 mg/g of wet cells for N122A, H190A, D58S, and D58N mutant enzymes, and 1 mg/g of wet cells for N122D mutant enzyme. The mutants D58T and D58E formed inclusion bodies.

Crystallization and X-ray Data Collection. Crystals were obtained at room temperature by vapor diffusion in hanging

Table 1: Data-Processing Statistics

space group	$C222_1$
cell dimension (Å)	$a = 90.0$, $b = 130.4$, $c = 90.5$
no. of molecules in the asymmetric unit	2
resolution (Å)	26.5−2.25
no. unique reflections	21,045
redundancy	5.2
completeness (%)[a]	83.3 (64.9)
R_{merge}[a,b]	0.064 (0.244)
$\langle I/\sigma(I)\rangle$[a]	13.8 (3.7)

[a] The values in parentheses are for the highest resolution shell, 2.29−2.25 Å. [b] $R_{merge} = \sum_{hkl}[(\sum_j|I_j - \langle I\rangle|)/\sum_j|I_j|]$ for equivalent observations.

drops. The protein drops were equilibrated against a reservoir solution containing 18% w/v poly(ethylene glycol) 4000, 15% glycerol, 5 mM $MgCl_2$, and 100 mM Hepes buffer (pH 7.0−8.0). The drops consisted of protein at a concentration of 9 mg/mL, and 5 mM S-pyr, diluted by an equal volume of reservoir solution.

For X-ray data collection, the crystal, in the mother liquor, was flash-cooled in liquid propane cooled by liquid nitrogen. Cu-Kα X-rays were supplied by a Siemens rotating anode generator. Diffraction intensity data were recorded on MAR345 imaging plate detector. Data were processed with HKL (*30*). The crystal belongs to space group $C222_1$, with unit cell dimensions $a = 90.0$ Å; $b = 130.3$ Å; $c = 90.5$ Å, parameters that are isomorphous with those of the enzyme/Mg(II)-oxalate crystal (*10*). Statistics of data processing are provided in Table 1.

Structure Determination and Refinement. The model of the enzyme/Mg(II)-oxalate structure (PDB entry code 1pym), omitting the Mg(II)-oxalate and solvent molecules, was used to calculate a difference Fourier map with the coefficients $2F_o - F_c$ and calculated phases (where F_o and F_c are the observed and calculated structure factors, respectively). The map revealed density for the bound Mg(II)-S-pyr, and a model was readily built.

The structure was refined at 2.25 Å resolution with the program CNS (*31*), first using simulated annealing at 3000 K, and then alternating positional and individual temperature factor refinement cycles. The two molecules of the asymmetric unit were refined independently. The progress of the refinement was evaluated by the improvement in the quality of the electron density maps, and the reduced values of the conventional R factor ($R = \Sigma_h||F_o| - |F_c||/\Sigma_h|F_o|$), and the free R-factor (6% of the reflections omitted from the refinement) (*32*). The electron density maps were inspected and the model modified on an interactive graphics workstation with the program O (*33*). Water molecules were added gradually as the refinement progressed. They were assigned in the $|F_o| - |F_c|$ difference Fourier maps with a 3σ cutoff level for inclusion in the model. The refinement statistics are shown in Table 2.

Steady-State Kinetic Measurements. The k_{cat} and K_m (for P-pyr) values for wild type and mutant PEP mutase were determined from initial velocity data. The rate of PEP formation in reactions containing PEP mutase, 5 mM $MgCl_2$, varying concentration of P-pyr (1−10-fold K_m), 50 mM K^+HEPES (pH 7.5, 25 °C), and the coupling system (1 mM ADP, 0.2 mM NADH, 10 unit/mL pyruvate kinase, and 10 unit/mL lactate dehydrogenase) was monitored by measuring the decrease in solution absorbance at 340 nm ($\Delta\epsilon = 6.2$ mM^{-1} cm^{-1}). The initial velocity data were analyzed using eqs 1 and 2 and the programs of Cleland (*34*). The K_i values for S-pyr and oxalate as competitive inhibitors vs P-pyr were calculated from eq 2 using initial velocity data measured in the presence and in the absence of S-pyr or oxalate.

Table 2: Refinement Statistics

resolution (Å)	26.5−2.25
unique reflections $F \geq 2\sigma(F)$	20235
completeness (%)	78.9
no. of protein atoms	4538
no. of water molecules	258
no. of Mg(II)-S-pyr	2
[a]R_{work}	0.179
[a]R_{free}	0.268
RMS deviation from ideal geometry	
bond length	0.009 Å
bond angle	1.5°
average B factor (Å^2)	
protein	35
H_2O	37
S-pyr	44
Mg(II)	27

[a] $R_{work} = \sum_{hkl}||F_o| - |F_c||/\sum_{hkl}|F_o|$, where F_o and F_c are the observed and calculated structure factors, respectively. R_{free} is calculated for randomly selected 6% of the reflections that were omitted from the refinement.

$$v_0 = V_m\,[S]/(K_m + [S]) \quad (1)$$

$$v_0 = V_{max}\,[S]/[K_m(1 + [I]/K_i) + [S]] \quad (2)$$

where v_0 = initial velocity, V_{max} = maximum velocity, [S] = substrate concentration, K_m = Michaelis constant for substrate, [I] = inhibitor concentration, and K_i = the inhibition constant.

For mutant proteins, k_{cat} values were calculated from V_m and enzyme concentration, [E], according to the equation $k_{cat} = V_{max}/[E]$, assuming that all active sites were active. Protein concentration was determined using the Bradford assay (*35*).

RESULTS AND DISCUSSION

S-pyr Is an Inhibitor of PEP Mutase. Sulfate monoesters are structurally similar to phosphate monoesters, but they have reduced charge (one vs two negative charges at physiological pH). Comparisons made between the solution chemistry of sulfate esters and phosphate esters have revealed close similarities in mechanisms and transition states (*36*). Nevertheless, sulfotransferases have evolved separately from phosphotransferases (*37*). In some cases, synthetic sulfate ester analogues of natural phosphate esters undergo catalyzed sulfuryl transfer by phosphotransferases but at substantially reduced efficiency (for example, sulfenolpyruvate and adenosine 5′-sulfatopyrophosphate are substrates of pyruvate kinase and nucleoside diphosphate kinase, respectively (*38*, *39*)). PEP mutase, while binding S-pyr tightly at the P−pyr binding site ($K_i = 22 \pm 1$ μM vs $K_i = 8.4 \pm 0.5$ μM measured for oxalate), does not catalyze the rearrangement of the S-pyr to sulfenolpyruvate.

Overall Structure. The final structure includes residues 5−295 of one molecule, and residues 5−293 of the second molecule of the asymmetric unit. The root-mean-square deviation (RMSD) between α-carbon atom positions of the

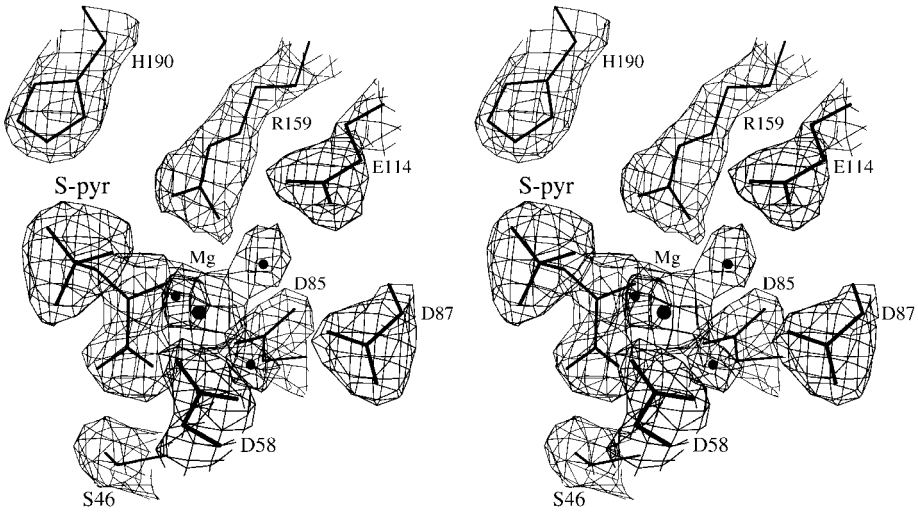

FIGURE 2: The electron density map at the active site, together with the final model. The coefficients $2F_o - F_c$ and calculated phases are used. The map is contoured at 1σ level.

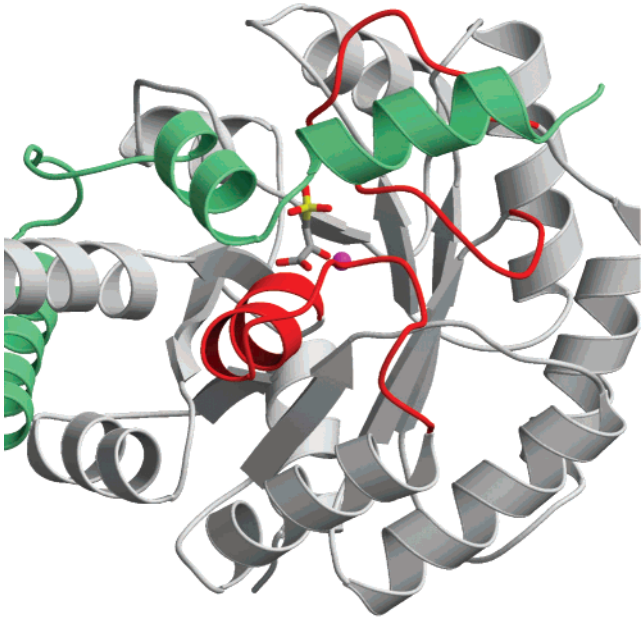

FIGURE 3: The location of Mg(II)-S-pyr binding site in PEP mutase. S-pyr is shown as a stick model. Atomic colors are as follows: oxygen − red, carbon − white, sulfur − yellow, Mg^{2+} − magenta. Structural units that prevent bulk solvent access to the active site are highlighted red (for the two loops on the same molecule), and green (for the neighboring molecule).

two molecules is 0.3 Å. The biological unit is a tetramer, which is generated by the crystallographic 2-fold symmetry axes. The Mg(II)-oxalate and Mg(II)-S-pyr bound protein structures are the same within the accuracy of the data resolution: The RMSD between α-carbon atom positions of the two structures is 0.2 Å. The pyruvyl unit of the S-pyr ligand occupies the same position observed for the oxalate. The electron density associated with the active site is shown in Figure 2.

PEP mutase biological unit is a dimer of intertwined dimers. Each molecule adopts an α/β barrel fold, with the barrel's eighth helix swapped between two molecules of the dimer. Each C-terminus segment (colored green in Figure 3) ensuing the eighth helix caps the active site of the partner molecule. Access to the active site is further blocked by two loops (colored red in Figure 3). The desolvation of the active site may be required to prevent PEP hydrolysis, while substrate binding and dissociation must be accompanied by conformational changes of the capping structural elements (*10*).

Mode of Inhibitor Binding. As with the Mg(II)-oxalate binding, and consistent with the usual mode of ligand binding to α/β barrel structures, the Mg(II)-S-pyr binds in a crevice at the center of the barrel, close to the carboxyl termini of the β strands (Figure 3). An identical binding mode is observed for the two molecules in the asymmetric unit. The inhibitor is isosteric with P-pyr, and hence the true reaction product is expected to bind in the same manner.

A rich network of interactions ensures the precise positioning of the S-pyr (Figure 4a). Mg(II) mediates inhibitor binding by forming octahedral coordination (average Mg− ligand distance of 2.2 Å) to a protein carboxyl group (Asp85), to two oxygen atoms of the pyruvate moiety of S-pyr (bidentate coordination to C(1)O and C(2)O), and to three water molecules, each of which is in turn hydrogen bonded to a protein carboxylate group (Asp58, Asp87, Glu114).

In addition to the coordination of S-pyr to Mg(II), the inhibitor interacts directly with the protein. The carboxylate group of the pyruvyl moiety is located in an oxyanion hole formed at the N-terminus of a short helix (not part of the α/β barrel framework), as does the carboxylate group of the oxalate inhibitor (Figure 1). One of the carboxylate oxygen atoms interacts with the two main chain NHs of Gly47 and Leu48, and the second carboxylate oxygen atom interacts with the hydroxyl group of a residue preceding the helix, Ser46.

Both the carbonyl oxygen atom and the sulfo oxygen atom of S-pyr interact with the guanidinium group of Arg159 (Figure 4a). The pyruvyl moiety is nonplanar, with a C1−C2 dihedral angle close to 60°, in contrast to the planar conformation of the oxalate inhibitor (Figure 1). The nonplanar pyruvyl group appears to facilitate the interaction between the sulfo group and the Arg159 side chain (otherwise, the two would point away from each other, and the sulfo group would form a much too close contact with the hydrophobic side chains of two residues, Val215, and Ala238). The two remaining oxygen atoms of the sulfo group also interact with protein side chains, one with Asn122, and

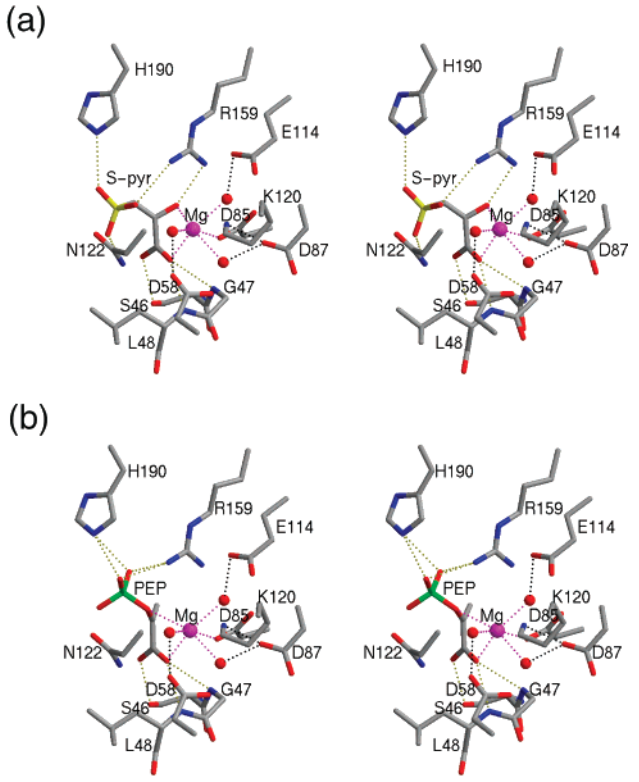

FIGURE 4: Active site interactions. Atomic colors are as in Figure 3. (a) Stereoscopic representation of the binding mode of S-pyr, highlighting key interactions with dotted lines. Coordination to the Mg(II) is shown in magenta, electrostatic interactions with S-pyr are shown in yellow, and protein interactions with Mg(II)-coordinated water molecules are shown in gray. (b) Stereoscopic representation of the binding mode of PEP, modeled based on the observed S-pyr binding mode. Color scheme for interactions is as in panel a.

Table 3: Steady-State Kinetic Constants Determined for Wild Type and Mutant PEP Mutase[a]

enzyme	k_{cat} (s^{-1})	K_m (μM)
wild-type	33.9 ± 0.4	1.6 ± 0.1
R159A	$1.0 \pm 0.1 \times 10^{-3}$	54 ± 2
D58A	no activity ($<1 \times 10^{-4}$)	
D58S	no activity ($<1 \times 10^{-4}$)	
D58N	$1.45 \pm 0.01 \times 10^{-2}$	7.8 ± 0.3
H190A	0.244 ± 0.001	6.5 ± 0.1
N122A	$6.00 \pm 0.08 \times 10^{-3}$	38 ± 1
N122D	$9.07 \pm 0.04 \times 10^{-3}$	3.2 ± 0.1

[a] Assays measured in 5 mM $MgCl_2$, pH 7.5, and at 25 °C.

the other with His190. Both of these residues are conserved among PEP mutase sequences, and their contributions to substrate binding and catalysis are examined in the following section.

Kinetic Properties of Active Site Mutants. The D58A mutant reported earlier was inactive. However, because the enzyme/S-pyr complex structure indicated that Asp58 is unlikely to serve as a phosphoryl acceptor, the function of this residue was further probed by site-directed mutagenesis. Two soluble mutants were generated, D58S and D58N. D58S is, within the limit of detection, inactive (Table 3). On the other hand, D58N is active but with reduced catalytic efficiency (k_{cat} is decreased 2000-fold and the K_m value is increased 5-fold).

In dehalogenases, which use an active site aspartate in covalent catalysis, slow conversion of the active site Asp → Asn mutant to wild-type enzyme occurs in buffer, and a comparatively rapid conversion occurs in the presence of the hydrolysis product (*40*, *41*). To test spontaneous conversion of the PEP mutase D58N mutant to wild-type enzyme, the activity of the D58N mutant was measured after a 1 h preincubation of the enzyme solution at 25 °C with 1 mM P-pyr or PEP, and after incubation for 10 days at 4 °C in buffer alone. No significant change in activity was observed. This result, together with the 5-fold larger K_m value, provides evidence that the low activity observed with the D58N mutant does not derive from contamination by the wild-type enzyme formed by hydrolysis of Asn58. Thus, catalysis proceeds, albeit at a reduced rate, in the absence of the Asp58 carboxylate. Since an asparagine is not a good nucleophile, the conclusion must be that the catalytic mechanism does not involve a phospho-aspartate intermediate.

The invariant residues, His190 and Asn122, whose side chains interact with the sulfo group of the bound S-pyr, were replaced by alanine residues, and for Asn122, a second mutant N122D was also prepared. The replacements at these two positions impair but do not eliminate catalysis (Table 3). The k_{cat} of the H190A mutant is 140-fold lower than that of wild-type PEP mutase, while the K_m value of the mutant is 4-fold greater than that of the wild-type enzyme. The retention of catalytic activity in the H190A mutant indicates that the histidine residue does not function as the phosphoryl group acceptor during PEP mutase catalysis. This conclusion is also compatible with an earlier finding for the PEP mutase from *Tetrahymena pyriformis*. Here it was shown that oxalyl phosphate, an alternate substrate for other PEP-dependent enzymes, does not react to form a phosphoenzyme species detected by isolation or by slow, tight binding inhibition (*8*). In contrast, the reaction of oxalyl phosphate with pyruvate phosphate dikinase, an enzyme that catalyzes phosphoryl transfer from PEP to an active site histidine during catalytic turnover, did result in the formation of a stable phospho-enzyme-Mg(II)-oxalate complex (*8*).

The amide group of Asn122 is not a likely candidate for a phosphoryl group acceptor. However, the possibility that Asn122 undergoes posttranslational conversion to aspartic acid, and that Asp122 functions as the phosphoryl acceptor, must be ruled out. The comparable reduction in k_{cat} values observed for the N122A and N122D mutants indicates that the native residue is indeed an asparagine, and that the Asn122 is important but not essential to catalysis. Asn122 and Asp58 are located on the two loops (colored red in Figure 3) that cover the active site during catalytic turnover. Asp58 mediates interactions between the two loops by interacting directly with Asn122 (invariant in PEP mutase sequences), and indirectly with the invariant Lys120 (via a Mg(II)-ligand water molecule). Thus, each of these three loop residues plays an important role in active site desolvation.

Mechanistic Implication. When the crystal structure of the PEP mutase/Mg(II)-oxalate complex was first determined, the main mechanistic question was whether Asp58 could serve as a phosphoryl group acceptor in a reaction that proceeds via a phosphoenzyme intermediate. The current structure, together with the observation that the D58N mutant enzyme is active, shows unambiguously that this is not the case. The inhibitor's sulfur atom is located nearly 6 Å away from the Asp58 carboxyl group. By analogy, the substrate's phosphorus atom would be much too far away for nucleo-

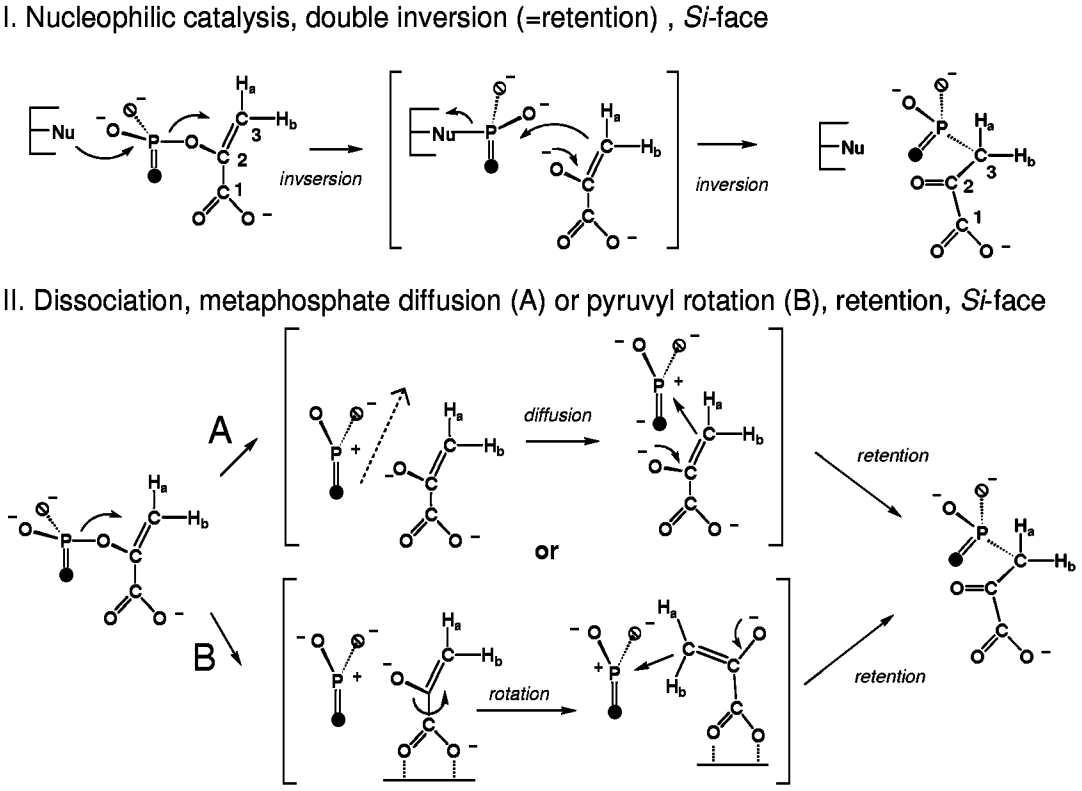

FIGURE 5: Dissociative pathways leading to retention of configuration in PEP mutase catalysis.

philic attack by Asp58. Instead, the position and the mutagenesis results indicate that Arg159, His190, and Asn122 may each be involved in electrostatic interaction with the phosphate oxygens but not form a covalent bond with the phosphorus.

How might dissociative phosphoryl transfer proceed in PEP mutase? The observed enzyme/S-pyr complex serves as a template to model the bound substrate, PEP (Figure 4b). Superposition of the pyruvyl group of PEP on that of S-pyr, while preserving the same C1−C2 dihedral angle value (approximately 60°), results in the phosphoryl group clashing with Arg159 and Mg(II). Counterclockwise rotation around the C1−C2 bond by approximately 110° relieves this clash, and positions the phosphoryl group so that, like the phosphonyl group, it forms favorable electrostatic interactions with the side chains of Arg159 and His190 (albeit with different orientation). Thus, the model suggests a reaction mechanism in which the metaphosphate dissociates from the pyruvyl unit of PEP (Figure 5). The metaphosphate's interactions with the protein hold it stationary, while the C1−C2 bond of the pyruvate enolate rotates before the C3−P covalent bond is formed. This mechanism requires minimal adjustments of active site residues, whereas the alternative dissociative mechanism, in which the pyruvate enolate is stationary and the metaphosphate diffuses from C(2)O to C(3), requires substantial changes to be made in the protein.

The structure of the PEP mutase in complex with Mg(II)-oxalate (Figure 1) may be considered a model of the reaction intermediate minus the metaphosphate (*10*). The increased electrostatic interaction that might take place between charged pyruvate enolate and the guanidinium group of Arg159, the Mg(II), and the oxyanion hole provides a significant source of stabilization.

We note that the counterclockwise rotation for the P-pyr to PEP transition is consistent with the reported *si* facial stereochemistry for the conversion of (*Z*)-phosphoenol-[3-D1]pyruvate to (*S*)-3-phosphono-[3-D1]-pyruvate (*42*), and with retention of configuration at the phosphorus. The high intrinsic energy of the metaphosphate formed accounts for the reported absence of detectable levels of trapped intermediate. Finally, a dissociative mechanism is also consistent with the similar substrate activity observed for phosphonopyruvate and thiophosphonopyruvate (*6*) and with the synergism in PEP mutase binding that occurs between oxalate and small planar anions (*7*).

In conclusion, the data presented in this paper show that in contrast to other phosphotransferases, which catalyze phosphoryl transfer with retention of configuration, PEP mutase does not employ a double-displacement mechanism. An alternate pathway, which is also compatible with the known stereochemistry at phosphorus and carbon, is proposed. In this mechanism, the phosphoryl group dissociates from the substrate to form metaphosphate and pyruvate enolate, and then reattaches following rotation about the pyruvyl C1−C2 bond.

ACKNOWLEDGMENT

The authors wish to thank Mike Gilson and Mo Cleland for helpful discussion.

REFERENCES

1. Bowman, E. D., McQueney, M. S., Barry, R. J., and Dunaway-Mariano, D. (1988) *J. Am. Chem. Soc. 110*, 5575−5576.
2. Seidel, H. M., Freeman, S., Seto, H., and Knowles, J. R. (1988) *Nature 335*, 457−8.
3. Seto, H., and Kuzuyama, T. (1999) *Nat. Prod. Rep. 16*, 589−96.

4. Bowman, E. D., McQueney, M. S., Scholten, J. D., and Dunaway-Mariano, D. (1990) *Biochemistry 29*, 7059−63.
5. Seidel, H. M., Freeman, S., Schwalbe, C. H., and Knowles, J. R. (1990) *J. Am. Chem. Soc. 112*, 8149−8155.
6. McQueney, M. S., Lee, S.-L., Swartz, W. H., Ammon, H. L., Mariano, S. M., and Dunaway-Mariano, D. (1991) *J. Org. Chem. 56*, 7121−7130.
7. Seidel, H. M., and Knowles, J. R. (1994) *Biochemistry 33*, 5641−6.
8. Kim, J., and Dunaway-Mariano, D. (1996) *Biochemistry 35*, 4628−35.
9. Kim, A., Kim, J., Martin, B. M., and Dunaway-Mariano, D. (1998) *J. Biol. Chem. 273*, 4443−8.
10. Huang, K., Li, Z., Jia, Y., Dunaway-Mariano, D., and Herzberg, O. (1999) *Structure Fold. Des. 7*, 539−48.
11. Jia, Y., Lu, Z., Huang, K., Herzberg, O., and Dunaway-Mariano, D. (1999) *Biochemistry 38*, 14165−73.
12. Cox, J. R., and Ramsay, B. (1964) *Chem. Rev. 64*, 317.
13. Westheimer, F. H. (1968) *Acc. Chem. Research 1*, 70.
14. Schray, K. J., and Benkovic, S. J. (1971) *J. Am. Chem. Soc. 93*, 2522−9.
15. Westheimer, F. H. (1981) *Chem. Rev. 81*, 313.
16. Knowles, J. R. (1980) *Annu. Rev. Biochem. 49*, 877−919.
17. Eckstein, F. (1983) *Angew Chem. Int. Ed. Engl. 22*, 423.
18. Frey, P. A. (1989) *Adv. Enzymol. Relat. Areas Mol. Biol. 62*, 119−201.
19. Cleland, W. W., and Hengge, A. C. (1995) *FASEB J. 9*, 1585−94.
20. Mildvan, A. S. (1997) *Proteins 29*, 401−16.
21. Hengge, A. C. (2001) *FEBS Lett. 501*, 99−102.
22. Ramirez, F., and Marecek, J. F. (1979) *J. Am. Chem. Soc. 101*, 1460.
23. Hoff, R. H., and Hengge, A. C. (1998) *J. Org. Chem. 63*, 195.
24. Gallagher, M. J., and Jenkins. (1968) in *Topics in Stereochemistry* (Eliel, E. L., and Allinger, N. L., Eds.) Wiley, New York.
25. Cleland, W. W. (1995) *Methods Enzymol. 249*, 341−73.
26. Friedman, J. M., Freeman, S., and Knowles, J. R. (1988) *J. Am. Chem. Soc 110*, 1268−1275.
27. Cullis, P. M., Misra, R., and Wilkins, D. J. (1987) *J. Chem. Soc. Chem. Commun. 1987*, 1594.
28. Anderson, V. E., Weiss, P. M., and Cleland, W. W. (1984) *Biochemistry 23*, 2779−86.
29. White, R. H. (1986) *Biochemistry 25*, 5304−5308.
30. Otwinowski, Z., and Minor, W. (1997) *Methods Enzymol. 276*, 307−326.
31. Brünger, A. T., Adams, P. D., Clore, G. M., DeLano, W. L., Gros, P., Grosse-Kunstleve, R. W., Jiang, J. S., Kuszewski, J., Nilges, M., Pannu, N. S., Read, R. J., Rice, L. M., Simonson, T., and Warren, G. L. (1998) *Acta Crystallogr. D Biol. Crystallogr. 54*, 905−21.
32. Brünger, A. T. (1992) *Nature 355*, 472−474.
33. Jones, T. A., Zou, J. Y., Cowan, S. W., and Kjeldgaard. (1991) *Acta Crystallogr. A 47*, 110−9.
34. Cleland, W. W. (1979) *Methods Enzymol. 63*, 103−38.
35. Bradford, M. M. (1976) *Anal. Biochem. 72*, 248−54.
36. Hengge, A. C. (2002) *Acc. Chem. Res. 35*, 105−12.
37. Negishi, M., Pedersen, L. G., Petrotchenko, E., Shevtsov, S., Gorokhov, A., Kakuta, Y., and Pedersen, L. C. (2001) *Arch Biochem. Biophys. 390*, 149−57.
38. Peliska, J. A., and O'Leary, M. H. (1989) *Biochemistry 28*, 1604−11.
39. Peliska, J. A., and O'Leary, M. H. (1991) *Biochemistry 30*, 1049−57.
40. Pries, F., Kingma, J., and Janssen, D. B. (1995) *FEBS Lett. 358*, 171−4.
41. Xiang, H., Dong, J., Carey, P. R., and Dunaway-Mariano, D. (1999) *Biochemistry 38*, 4207−13.
42. Hammerschmidt, F., and Kahlig, H. (1992) *Liebigs Ann. Chem. 1992*, 1201−1203.

BI026024V